APPLIED ORGANOMETALLIC CHEMISTRY
*Appl. Organometal. Chem.* 2003; **17**: 42–51
Main Group Metal Compounds AOC
Published online in Wiley InterScience (www.interscience.wiley.com). DOI:10.1002/aoc.382

# Order–disorder phenomena in crystalline phases of compounds $E(XMe_3)_4$ where E = C, Si, Ge and X = Si, Sn

**Xavier Helluy and Angelika Sebald***

Bayerisches Geoinstitut, Universität Bayreuth, 95440 Bayreuth, Germany

Received 20 June 2002; Accepted 4 August 2002

**We discuss the dynamic solid-state properties of crystalline phases $E(XMe_3)_4$ as seen by solid-state NMR and powder X-ray diffraction. In the first part we will qualitatively describe some of the NMR tools suitable for such investigations. In the second part we will give examples from the group of solid compounds $E(XMe_3)_4$ with E = C, Si, Ge and X = Si, Sn. Copyright © 2002 John Wiley & Sons, Ltd.**

**KEYWORDS:** dynamic disorder; organometal compounds; solid-state NMR; powder X-ray diffraction

## INTRODUCTION AND OUTLINE

We describe the picture emerging from combined high-resolution powder X-ray diffraction and solid-state NMR studies about structure and dynamics of a series of organometallic compounds, highlighting the advantages in the combined use of these two complementary experimental techniques. We will focus on a particular class of compounds, $E(XMe_3)_4$, where E = C, Si, Ge and X = Si, Sn. In the solid state their crystal lattices are built from non-polar molecular building blocks; this class of solid compounds displays a multitude of order–disorder phenomena. For most members of this series of compounds it turns out to be difficult to impossible to obtain single crystals suitable for X-ray diffraction studies. Hence, studies of the structure and dynamics of these solid phases have to be carried out on polycrystalline powders.

The next section briefly summarizes the various possible modes of dynamic disorder in these compounds. Some of these dynamic processes cannot be seen by X-ray diffraction experiments, whereas others are not accessible to high-resolution solid-state NMR techniques. The third section will outline the experimental solid-state NMR tools for characterizing and quantifying (some of) the dynamic processes occuring in these solid materials. The fourth section will deal with the results obtained on the series of solid compounds $E(XMe_3)_4$ and will attempt to provide an overview rather than detailed information; for detailed descriptions of studies of the individual compounds in this series the reader is referred to the literature.[1–4]

*Correspondence to: A. Sebald, Bayerisches Geoinstitut, Universität Bayreuth, 95440 Bayreuth, Germany.
E-mail: angelika.sebald@uni-bayreuth.de
Contract/grant sponsor: Deutsche Forschungsgemeinschaft.
Contract/grant sponsor: Aventis, Paris.

## DYNAMIC PROCESSES IN SOLID COMPOUNDS $E(XME_3)_4$

Disorder in solid materials may be of a static or a dynamic nature (or, in fact, sometimes both). An example for static disorder would be lack of long-range order in materials such as glasses. Here we will be solely concerned with thermally activated dynamic disorder phenomena in crystalline materials. Dynamic disorder may primarily affect the long-range order of the material and lead to structural phase transitions, with the degree of order increasing with decreasing temperatures. The primary effect may also be affecting the short-range order more than the long-range order, examples being the reorientation of molecules or molecular subunits by occasional jumps between equivalent positions in the crystal lattice. Of course, there are borderline areas between these two extremes. Dynamic solid-state disorder is a very natural area for joint investigations by diffraction and spectroscopic methods such as solid-state NMR, since diffraction techniques are most sensitive to long-range order and the strength of NMR spectroscopy is in the short-range domain.

The dynamic solid-state properties of the series of chemically homologous compounds $E(XMe_3)_4$, with E = C, Si, Ge and X = Si, Sn as seen by both X-ray diffraction and solid-state NMR will serve as an illustrative example. Fig. 1 summarizes those dynamic disorder modes in solid compounds $E(XMe_3)_4$ at the molecular level which are accessible

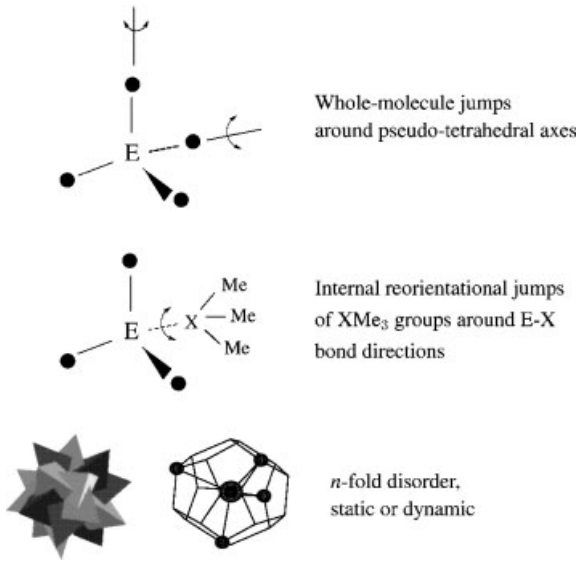


**Figure 1.** Schematic illustration of the different exchange processes in compounds $E(XMe_3)_4$. The pentagonal dodecahedron (bottom part) symbolises fivefold orientational disorder. In addition to the processes shown, the $CH_3$ groups themselves undergo internal reorientation at usually fast rates. Throughout the text we will assume fast $CH_3$-group internal reorientation.

to quantitative study by the solid-state NMR techniques explained in the following section. These exchange processes include whole-molecule jumps around the molecular pseudo-tetrahedral axis, internal reorientation of all or some of the $XMe_3$ groups in the molecule around the E—X bond directions, and *n*-fold orientational disorder of the entire molecule in the crystal lattice. Since all our NMR probes here will be isolated spin-1/2 nuclei, the exchange processes will affect the solid-state NMR spectra as follows. The methyl $^{13}C$ resonances of the $XMe_3$ groups will be affected by all three kinds of dynamic disorder. Internal reorientation of the $XMe_3$ groups will affect only the respective interchanging methyl $^{13}C$ resonances, not the NMR resonances of E and X. The resonances of E and X are both affected by *n*-fold orientational disorder and the X resonances by whole-molecule reorientational jumps, and thus they can serve as NMR probes for studying and distinguishing these processes.

## EXPERIMENTAL NMR TOOLS FOR STUDYING SOLID-STATE DYNAMICS

The study of dynamic processes in solid materials is a classical area of solid-state NMR applications, dating back to the early days in the history of this experimental technique.[5,6] The strength of solid-state NMR techniques in this application area rests on the wide range of rate constants that are accessible to a quantitative study by means of various different NMR techniques. Kinetic data, recorded by NMR as a function of temperature, yield activation energies of thermally activated processes in solids.

Fast(er) motional processes in solids can be studied by relaxation measurements and/or other wideline techniques, such as deuterium NMR experiments on non-spinning powder samples. Though valuable quantitative data on the kinetics (and energetics) of motional processes in solids are accessible in this way, these NMR techniques usually do not provide a direct and unambiguous fingerprint as to the precise nature of the dynamic process that is being monitored. In the slow motional regime, NMR experiments can deliver not only quantitative data on kinetic parameters but also unambiguous evidence about the nature of the ongoing exchange process. When speaking about 'slow' or 'fast' exchange regimes we refer to the time scales monitored by a given NMR experiment. Of course, temperature-variation NMR experiments play an important role in shuttling through and between these exchange regimes and in providing the basis for the determination of activation barriers of thermally activated processes.

Here we concentrate on those solid-state NMR techniques which give direct insight into exchange processes in solids and also depict the geometry of an exchange process. The relevant range of rate constants will be of the order $10^0$ to $10^4$ $s^{-1}$. By limiting our consideration to this 'high-resolution' regime of relatively slow dynamic processes, we trade a limited range of accessible rate constants against the unique quality of the information accessible in this regime. There are essentially three different types of solid-state NMR experiment that form the basis of investigations on solid-state dynamics by observation of isolated spin-1/2 nuclei. In fact, the availability of spin-1/2 isotopes at low natural abundance is an important ingredient in these types of NMR experiment. While dipolar coupled, extended clusters of spin-1/2 nuclei are a particularly rich source of information in the quantitative determination of structural parameters such as internuclear distances or molecular torsion angles by means of so-called dipolar recoupling experiments (for general review articles on recoupling methods under Magic-angle spinning (MAS) NMR conditions, see Refs 7 and 8), in the context of molecular solid-state dynamics the presence of additional NMR interaction tensors such as dipolar coupling often adds intractable complications: NMR experiments capable of depicting the effects of *molecular* exchange also depict the effects of simultaneous *spin* exchange (spin diffusion) occurring in dipolar coupled spin systems.[9] These combined effects would often be hopeless cases in terms of extracting the contributions arising solely from the molecular dynamics. Obviously, the argument also applies in the other direction: when aiming to determine structural parameters from solid-state NMR experiments on dipolar coupled spin systems, the presence of dynamic processes adds tremendous complications or, in fact, might be a severe source of error if not taken into account.

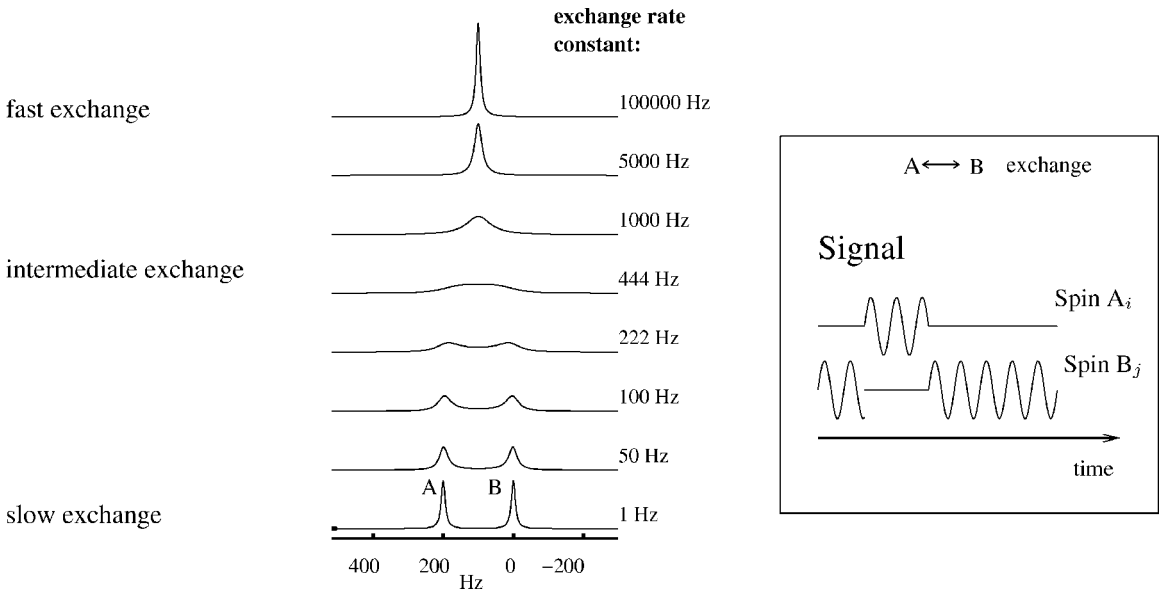


**Figure 2.** The effects of mutual exchange on one-dimensional MAS NMR spectra (left part); calculated spectra for a two-site exchange as a function of the exchange-rate constant are shown. At the right, we symbolize the exchange amongst spin packages, which is the physical basis of the exchange effects monitored in the NMR spectra.

In the first experimental scenario we assume MAS of the sample, at an MAS frequency exceeding the spread of the chemical shielding tensors. We further assume two inequivalent sites in the sample amongst which exchange takes place. Such MAS NMR spectra as a function of the exchange rate constant are shown in Fig. 2 for a two-site exchange. This situation is equivalent to monitoring a two-site exchange process in solution-state NMR, including the extraction of the exchange rate constants as a function of temperature by simulations, based on an exchange-matrix formalism.[9,10] What has to be considered as slow, intermediate and fast exchange in this one-dimensional approach is governed by the isotropic chemical shift difference $\Delta\omega_{iso}$ (Hz). Obviously, the Larmor frequency of the observed nucleus plays a role, and $\Delta\omega_{iso}$, to some extent, is under experimental control by the choice of the external magnetic field strength. The temperature range which guides the one-dimensional MAS exchange-affected spectra from the one-dimensional slow-exchange regime to the one-dimensional fast-exchange regime then depends on (i) the absolute rate constants of the process, and (ii) the activation energy of the process. The lower the activation energy, the larger is the temperature range which promotes the spectra from the slow-exchange to the fast-exchange regime. Between these two regimes, the lineshapes are sensitive to the exchange rate constants and may be used to extract these values, as a function of temperature, from experimental spectra.

Note the following general points concerning this experimentally straightforward one-dimensional MAS NMR approach. The underlying exchange-matrix formalism is easily extended from the simple two-site case to more complicated cases where exchange amongst more sites occurs. Recording one-dimensional variable-temperature MAS NMR spectra for subsequent lineshape analysis obviously requires the exchange to take place amongst crystallographically inequivalent sites giving rise to spectrally resolved resonances in the slow-exchange limit (alternative MAS NMR experiments exist which permit monitoring chemical exchange amongst crystallographically equivalent sites via isolated spin-1/2 nuclei in one-dimensional experiments;[11,12] see below). The convenient MAS regime, where only isotropic chemical shielding needs to be taken into account for the data analysis, is most easily met for spin-1/2 isotopes in sites giving rise to modest chemical shielding anisotropies, examples being the $^{13}C$ resonances of methyl groups, or $^{29}Si$ resonances of $SiMe_3$ groups. It is not a trivial task to determine precisely the absolute temperature inside a spinning rotor, despite some existing calibration methods.[13–15] Hence, it may be wiser to consider only the slope of Arrhenius plots derived from MAS NMR experiments and not to emphasize any pre-exponential factors. Lineshape calculations of exchange-broadened MAS NMR spectra are not an entirely model-free approach: a specific exchange model is the starting point in setting up the calculations. Another effect has to be taken into account in the analysis procedure. Isotropic chemical shielding displays small intrinsic temperature shifts to either higher or lower frequencies as a function of temperature. These intrinsic temperature shifts have to be taken into account, especially when dealing with data obtained over a large temperature range.

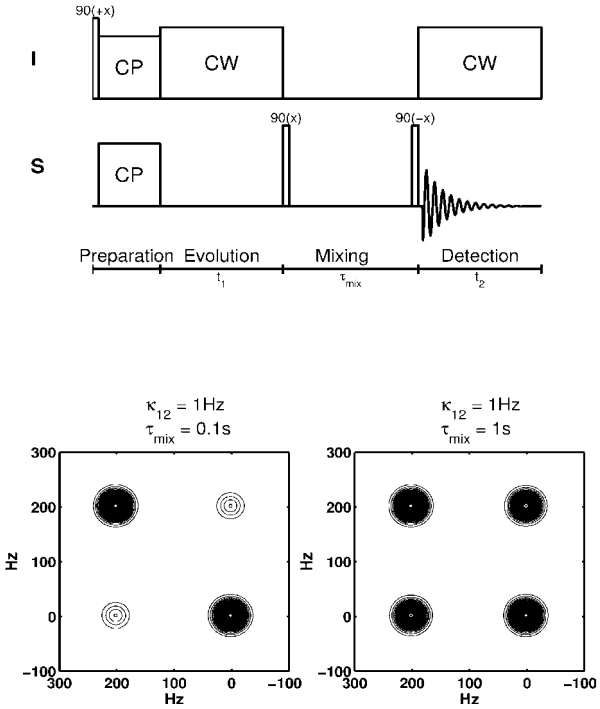


**Figure 3.** 2D EXSY spectroscopy under fast-spinning MAS conditions. Top: the pulse sequence. Bottom: calculated contour plots of 2D EXSY experiments of a two-site exchange with an exchange rate constant $\kappa_{12}$ = 1 Hz, where (left) a short mixing time $\tau_{mix}$ = 0.1 s and (right) a long mixing time $\tau_{mix}$ = 1 s is assumed. The diagonal peaks correspond to the two isotropic chemical shielding values of the two exchanging sites.

Our second scenario maintains the above-mentioned fast-spinning MAS regime, where only isotropic chemical shielding needs to be taken into account. As is seen in Fig. 2, low temperatures — or, rather, small exchange rate constants — leave the MAS NMR lineshapes largely unaffected by exchange process(es). In this regime, extending the range of accessible exchange rate constants to slower processes, two-dimensional (2D) exchange spectroscopy (EXSY) is the method of choice.[9,16] The pulse sequence and contour plots of calculated spectra, again for a two-site exchange, are shown in Fig. 3. Here, information about exchange rate constants is directly encoded in the relative intensities of the off-diagonal peaks. Thus, extraction of exchange rate constants from 2D EXSY experiments is a truly model-free procedure. In addition, the connectivity of different sites by mutual exchange is directly displayed in the resulting contour plots by the absence or presence of cross peaks. This not only greatly extends the range of accessible exchange rate constants to much lower values, it represents a considerable additional gain in specific information compared with solely inspecting variable-temperature one-dimensional MAS NMR spectra. In that respect, the 2D EXSY approach under MAS conditions is again closely related to its solution-state NMR counterpart. The limit for the maximum duration of the mixing time $\tau_{mix}$ is ruled by the $T_1$ relaxation of the observed nucleus. Thus, for 2D EXSY experiments on solids it is a favourable circumstance that usually these $T_1$ relaxation times are long, much longer than in solution, and thus very slow dynamic processes are observable. Commonly, it is necessary to carry out a series of 2D EXSY experiments, at different temperatures and with different durations of $\tau_{mix}$. Depending on the sample at hand, this may require nontrivial amounts of spectrometer time. Where necessary, it is also possible to extend 2D EXSY experiments to a dynamic regime where the exchange process no longer leaves the one-dimensional lineshapes unaffected. In this regime of slightly faster exchange, the analysis of 2D EXSY experiments becomes a little bit more involved and requires full simulations rather than just integration of the cross-peak intensities.[16] Sometimes it is necessary to ensure that the experimentally observed cross peaks are not the result of so-called $^1$H-driven spin diffusion[17] but of molecular dynamics. Since $^1$H-driven spin diffusion can be quenched by applying high-power $^1$H decoupling during $\tau_{mix}$ (see Fig. 3), a comparison of 2D EXSY experiments with and without $^1$H decoupling applied during $\tau_{mix}$ permits this distinction. Note, however, that extended periods of high-power $^1$H decoupling, in excess of a few hundred milliseconds, are not advisable.

The third experimental scenario is specific to the solid state and has no direct counterpart in solution-state NMR. Now MAS is omitted and we deal with the broad, so-called powder patterns in solid-state NMR spectra of nonspinning polycrystalline samples. As before, we consider isolated spin-1/2 nuclei. Chemical shielding is an anisotropic property which is described mathematically be a second-rank tensor. Each crystallite orientation in a powder sample adds a specific chemical shielding value in a conventional NMR spectrum, resulting in the usually broad powder pattern arising from chemical shielding anisotropy (CSA) in the absence of molecular dynamics and MAS (see Plate 1a)). For isolated spin-1/2 nuclei, this powder pattern is fully described by just the three eigenvalues of the chemical shielding tensor, and in the general case no information regarding the orientation of the chemical shielding tensor in the molecular (or crystal) frame is encoded in the CSA-powder pattern of an isolated spin-1/2 nucleus in a powder sample. Often, however, the orientation in the molecular frame is either known from other NMR experiments or can be assumed with sufficient confidence.

Take a two-site exchange in a molecule undergoing a reorientational jump such that the CSA orientations of the two exchanging sites are different with respect to the magnetic field direction. This corresponds to a specific set of angles relating the directions of the two chemical shielding tensor principal axes before and after the jump. Note that this set of angles is the same for each crystallite/

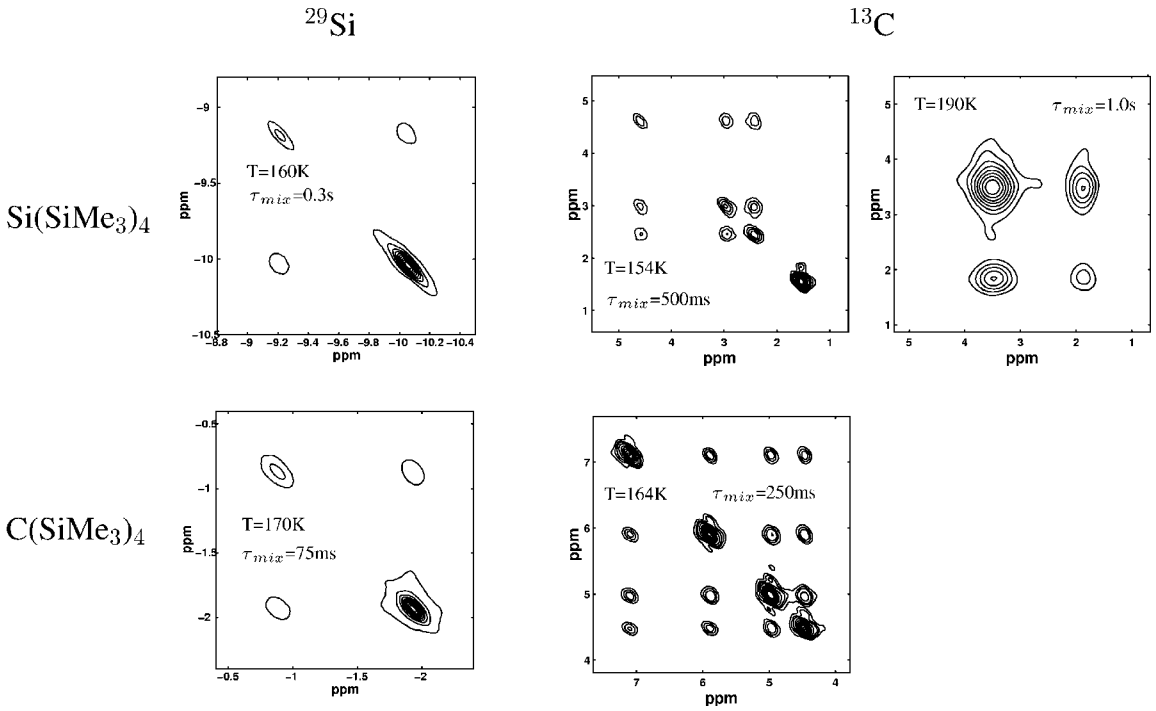


**Figure 4.** Contour plots of 2D EXSY MAS spectra of the low-temperature phases of $Si(SiMe_3)_4$ (top) and $C(SiMe_3)_4$ (bottom); experimental conditions are indicated. At the left, contour plots of $^{29}$Si 2D EXSY MAS spectra demonstrate whole-molecule reorientation occuring in both compounds. At the right, contour plots of $^{13}$C 2D EXSY MAS spectra are shown, with short and long mixing times for $Si(SiMe_3)_4$ in the top row. See Ref. 1 for further details.

molecule orientation in the powder sample. Different crystallite orientations will, as before in the absence of motion, contribute 'their part' to the powder pattern. But the presence of an exchange process will now correlate parts of the powder pattern with each other, according to the specific set of angles relating the two interchanging chemical shielding tensor directions (see Plate 1b)). Suppose the exchange process is slow on a time scale defined by the spread of the chemical shielding tensors (of the order of $10^2$ to $10^5$ Hz). A 2D EXSY experiment, recorded on a nonspinning powder sample under these slow-exchange conditions, thus permits one to map out the exchange amongst different CSA orientations or, in somewhat more unusual disorder cases, it may be used to track biased populations in orientationally disordered phases.[18] If the orientation of the chemical shielding tensor(s) in the molecular frame is known, the angular values describing the geometry of the mutual exchange between the chemical shielding tensors bear a direct relationship to the molecular geometry/jump angle of the exchange process. This 2D EXSY approach on nonspinning powder samples also works for exchange between crystallographically equivalent sites, with equal chemical shielding tensor eigenvalues of the mutually exchanging chemical shielding tensors but differing CSA orientations. We have now added some complexity to the analysis procedure, in that calculations/simulations have to include CSA orientations and powder averaging, but we have gained additional information not available from the previously described techniques. First, we have added another time scale of observation: the time scale corresponding to the spread of the CSA tensors becomes accessible. In addition, we now have a complete and direct fingerprint of the geometry involved in a dynamic exchange process. Typically, in contour plots of 2D EXSY spectra of nonspinning samples, different jump angles give rise to characteristic ridges, with small jump angles leading to features near the diagonal and large jump angles corresponding to ellipsoid features stretching away from the diagonal. Mainly for reasons of signal-to-noise ratio achievable within reasonable amounts of spectrometer time, it may sometimes be preferable to perform 2D EXSY experiments not on a nonspinning sample, but on a slowly spinning sample (where 'slow' is defined as considerably less than the spread of the chemical shielding tensor). Under slow-spinning MAS conditions, either one-dimensional MAS NMR experiments monitoring exchange amongst crystallographically equivalent sites[11,12] or 2D EXSY experiments may be performed; the latter then need to be performed in a rotation-synchronized manner.[19,20]

We may now proceed and have a look at the results obtained by such solid-state NMR experiments in conjunction with high-resolution powder X-ray diffraction studies

 

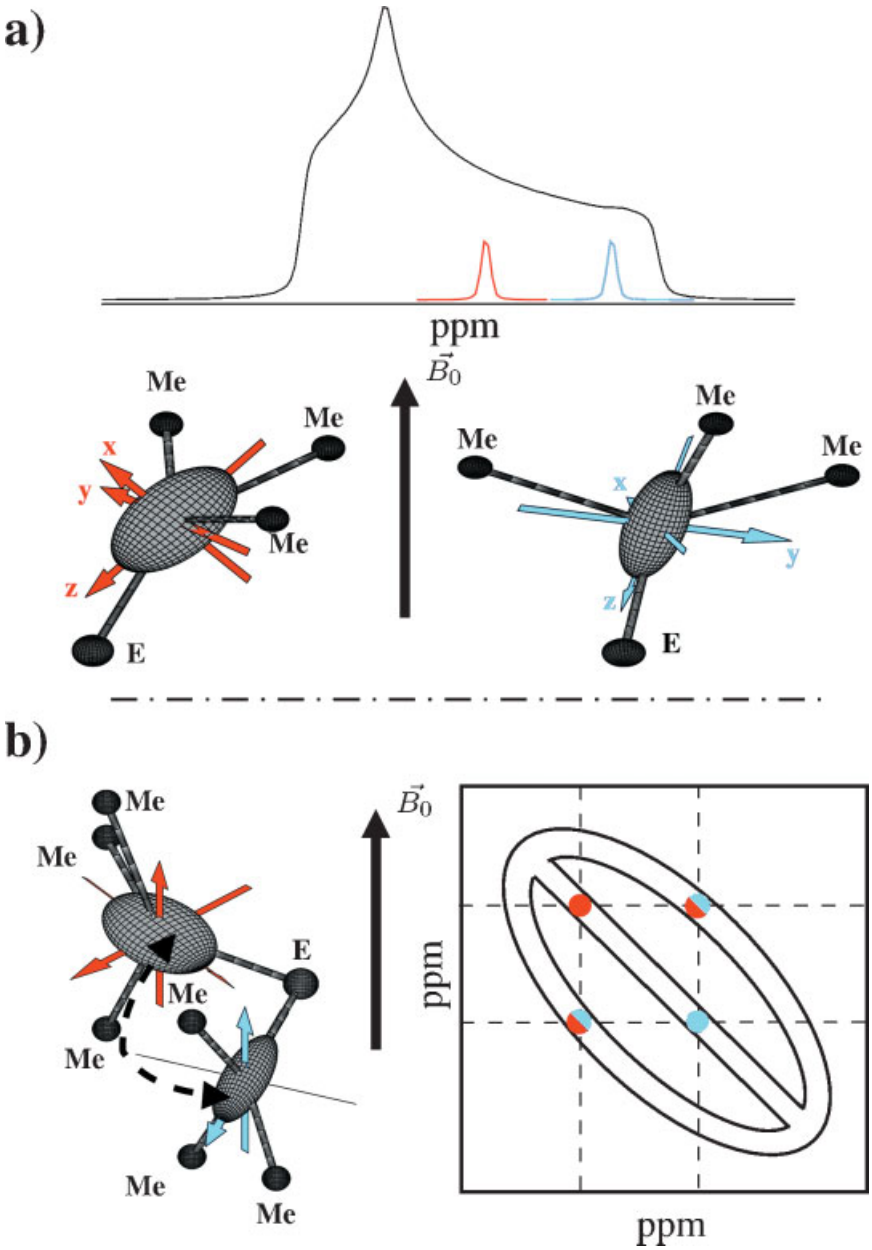


**Plate 1.** 2D EXSY spectroscopy on nonspinning powder samples; the pulse sequence is identical to the sequence shown in Fig. 3. (a) Two different crystallite orientations of a symbolic E—$XMe_3$ fragment in the absence of exchange amongst the two sites, with the directions of the X-spin chemical shielding tensor principal values indicated as *x,y,z* in red and blue for the two orientations; also shown is the entire powder spectrum of the X spins in the sample, with the individual contributions originating from the crystallite orientations of the 'red spin' and the 'blue spin' indicated. (b) The effects of a two-site exchange amongst the 'blue site' and the 'red site' as depicted in a symbolic contour plot of a 2D EXSY experiment on a nonspinning powder sample. The powder pattern from the one-dimensional experiment is now represented by the diagonal in the contour plot, while exchange processes affecting the chemical shielding tensor orientations lead to ellipsoid ridges in the contour plot. The precise shape of these ellipsoid features reflects the set of angles describing the mutual orientation of the two exchanging chemical shielding tensors (see Fig. 7 for realistic examples).

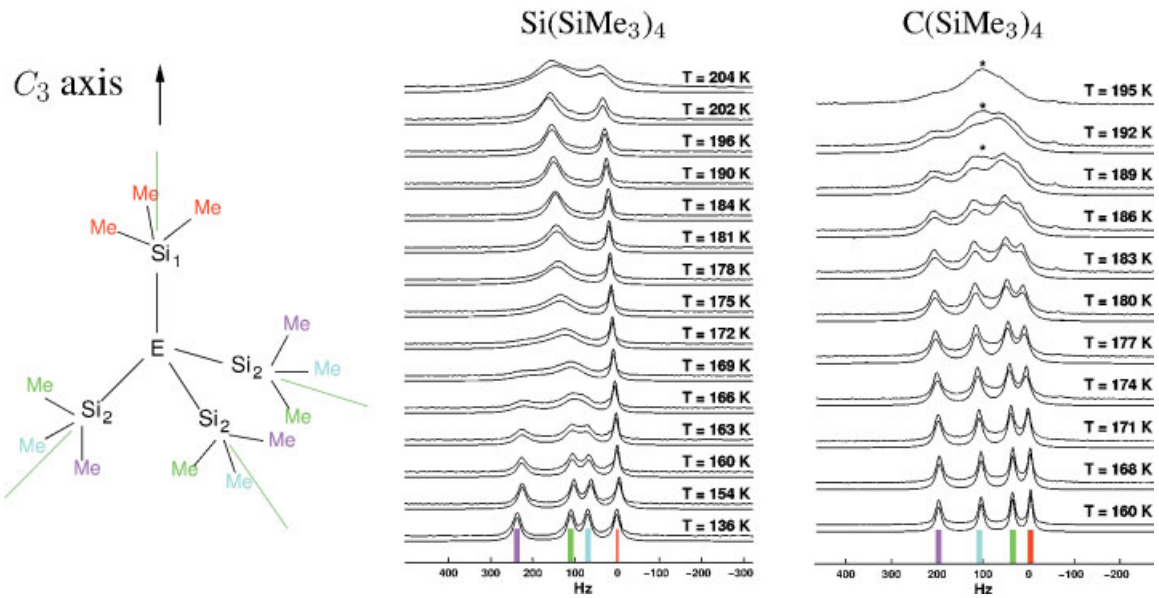


**Plate 2.** $^{13}C$ variable-temperature MAS NMR spectra of the low-temperature phases of $Si(SiMe_3)_4$ (left) and $C(SiMe_3)_4$; top traces are experimental spectra; bottom traces are the corresponding best-fit simulated spectra. In both cases the molecular symmetry is $C_3$; assignment of the various resonances into groups is indicated by colour codes. In the experimental $^{13}C$ MAS spectra of $C(SiMe_3)_4$ at $T > 189$ K, the star symbols mark the emerging $^{13}C$ resonance due to the beginning coexistence of the intermediate-temperature phase. See Ref. 1 for further details.

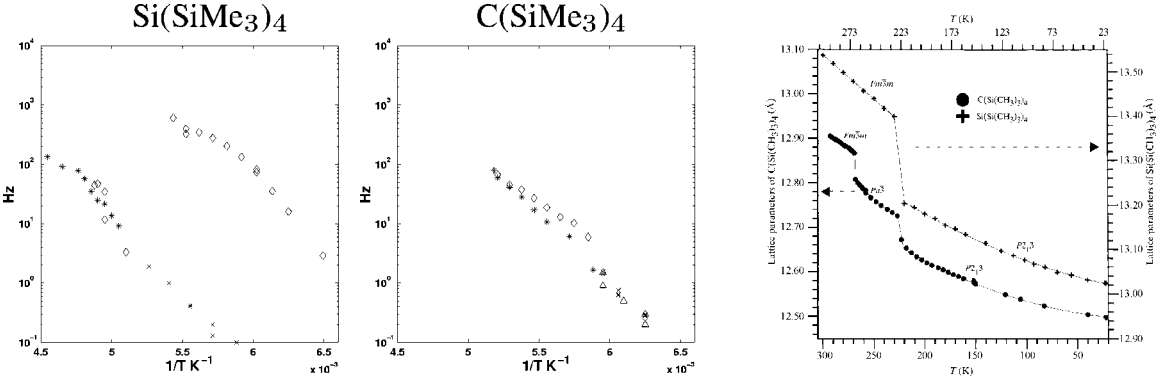


**Figure 5.** Summary of all exchange rate constants obtained from $^{13}C$ and $^{29}Si$ MAS NMR experiments on $Si(SiMe_3)_4$ (left) and $C(SiMe_3)_4$ (middle), as well as a plot of the crystallographic unit cell parameters as a function of temperature (right). The symbols give exchange rate constants obtained from one-dimensional $^{13}C$ (diamonds) and $^{29}Si$ (stars) MAS experiments, and from $^{13}C$ (triangles) and $^{29}Si$ (crosses) 2D EXSY MAS experiments. See Refs. 1 and 2 for further details.

on the dynamic solid-state properties of compounds $E(XMe_3)_4$.

## DYNAMIC PROPERTIES OF SOLID COMPOUNDS $E(XME_3)_4$ WITH E = C, SI, GE AND X = SI, SN

### $Si(SiMe_3)_4$ and $C(SiMe_3)_4$

The dynamic properties of the low-temperature phases of $Si(SiMe_3)_4$ and $C(SiMe_3)_4$ as seen by variable-temperature one- and two-dimensional $^{13}C$ and $^{29}Si$ MAS NMR are illustrated in Plate 2 and Fig. 4. For these two compounds, MAS NMR experiments relying solely on information from isotropic $^{13}C$ and $^{29}Si$ chemical shielding effects are sufficient to characterize the molecular dynamics. There is only one possibility to explain all experimental NMR and powder X-ray diffraction data obtained on these two compounds. In both cases in the respective low-temperature phase there is one orientationally ordered molecule in the asymmetric unit, displaying $C_3$ point group symmetry. Both $Si(SiMe_3)_4$ and $C(SiMe_3)_4$ undergo whole-molecule jumps around their main molecular axis, leading to intramolecular exchange of the various $SiMe_3$ groups. The two compounds differ, however, regarding internal reorientation of the various $SiMe_3$ groups themselves. Internal $SiMe_3$-group reorientation takes place in the low-temperature phase of $Si(SiMe_3)_4$ with an activation barrier similar to that of the whole-molecule reorientation, while internal $SiMe_3$-group reorientation is absent in the low-temperature phase of $C(SiMe_3)_4$. These similarities and differences in the dynamic properties are easily recognized and quantified in various one-dimensional (Plate 2) and two-dimensional (Fig. 4) $^{13}C$ and $^{29}Si$ MAS NMR experiments. The absence of internal $SiMe_3$-group reorientation in $C(SiMe_3)_4$ may be qualitatively explained by more pronounced intramolecular steric crowding compared with $Si(SiMe_3)_4$. Not only the molecular dynamic properties of $Si(SiMe_3)_4$ and $C(SiMe_3)_4$ differ from each other, but also their structural phase transition properties are different. These differences in molecular dynamics and phase transition properties are summarized in Fig. 5. $Si(SiMe_3)_4$ proceeds directly from its room-temperature phase (space group $Fm\bar{3}m$) to its low-temperature phase (space group $P2_13$). In contrast, $C(SiMe_3)_4$ reaches its low-temperature phase (again space group $P2_13$) from its room-temperature phase (again space group $Fm\bar{3}m$) only via an intermediate phase with space group $Pa\bar{3}$. A full account of the solid-state properties of $Si(SiMe_3)_4$ and $C(SiMe_3)_4$ is given elsewhere.[1,2]

### $C(SnMe_3)_4$

$C(SnMe_3)_4$ is the only compound in our series of compounds $E(XMe_3)_4$ for which the single-crystal X-ray diffraction structure is known.[21] At ambient conditions $C(SnMe_3)_4$ crystallizes in space group $Pa\bar{3}$ and displays five fold orientational disorder, whereby it was undetermined if the orientational disorder is of a static or dynamic nature. The intermediate-temperature phase of $C(SiMe_3)_4$ also crystallizes in space group $Pa\bar{3}$, though with only two fold orientational disorder.[2] Hence, our initial motivation for studying the properties of $C(SnMe_3)_4$ was viewing this compound as a slowed-down model of the solid-state dynamics of the intermediate-temperature phase of $C(SiMe_3)_4$, which itself is not suitable for in-depth solid-state NMR investigations of this kind as all the molecular dynamics in this phase are too fast for this purpose.[2]

The variable-temperature $^{119}Sn$ NMR spectra $C(SnMe_3)_4$ depicted in Fig. 6 demonstrate the presence of dynamic exchange processes in solid $C(SnMe_3)_4$, affecting the anisotropic $^{119}Sn$ chemical shielding. The $^{119}Sn$ CSA observed for $C(SnMe_3)_4$ is inconveniently small for applying

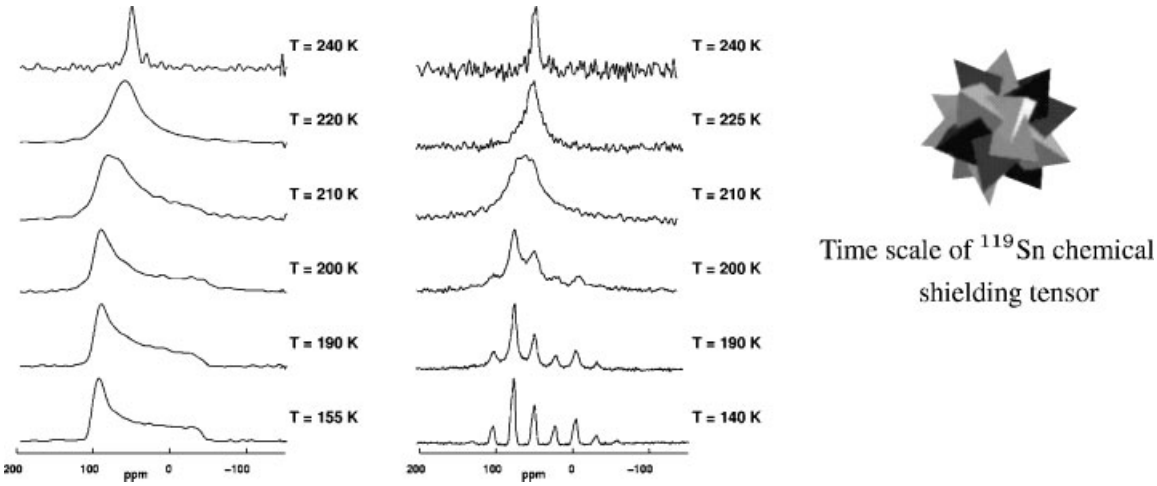


**Figure 6.** Variable-temperature $^{119}$Sn NMR experiments on $C(SnMe_3)_4$. Left: nonspinning sample; right: slow-spinning MAS conditions. Note the coalescence regime affecting the anisotropic $^{119}$Sn chemical shielding. See Ref. 3 for further details.

EXSY experiments under slow-spinning conditions. Since there are no spectrally resolved $^{119}$Sn resonances, here the $^{119}$Sn 2D EXSY experiments performed on a nonspinning sample of $C(SnMe_3)_4$ at low temperatures are the method of choice. The top parts of Fig. 7 illustrate which type of dynamic disorder processes would give rise to which kind of $^{119}$Sn 2D EXSY spectra. The first row depicts pictorial representations of different possible disorder models for $C(SnMe_3)_4$. Model (a) represents the situation where the orientational disorder is static but where whole-molecule jumps occur without the individual molecules in the crystal lattice changing their orientation. The following three models (b) to (d) refer to situations where both large-angle jumps (whole-molecule reorientation) and small-angle jumps occur simultaneously and where, over time, each tin atom visits each of the 20 corners of a pentagonal dodecahedron. In this situation, the exchange rate constants for both large- and small-angle jumps could be equal (model (b)) or differ from each other (models (c) and (d)). Finally, the model situation (e) depicted to the right corresponds to a completely isotropic reorientation. The second row in Fig. 7 shows simulated contour plots of 2D EXSY experiments as one would expect them for the various dynamic disorder models (a) to (e) when using mixing times $\tau_{mix}$ long enough to ensure complete exchange. Obviously, with long mixing times the 2D EXSY experiments can easily distinguish cases (a), (e) and (b)–(d) from each other, but finer distinctions within the different 20-site exchange cases (b)–(d) are not possible; they all result in identical full-exchange patterns. However, these distinctions can be made when using 2D EXSY experiments with short mixing times $\tau_{mix}$ in addition. This can be seen from the simulated 2D EXSY contour plots in the third row of Fig. 7. The bottom part of Fig. 7 depicts experimental and best-fit simulated $^{119}$Sn 2D EXSY experiments on $C(SnMe_3)_4$; the model which fits best all experimental data is model (b), where 20-site exchange of the tin sites occurs with equal exchange rate constants for small- and large-angle jumps. This analysis includes one assumption: we have assumed that the directions of the unique (here most shielded) components of the $^{119}$Sn chemical shielding tensors in $C(SnMe_3)_4$ are oriented along the $Sn-C_{central}$ bond directions. Finally, it turns out that $C(SnMe_3)_4$ does not seem to be a particularly suitable model of the dynamic properties of the intermediate-temperature phase of $C(SiMe_3)_4$ since $C(SnMe_3)_4$ does not undergo a phase transition to an orientationally ordered low-temperature phase, at least not at temperatures above $T = 30$ K. A full account of the solid-state properties of $C(SnMe_3)_4$ is given elsewhere.[3]

## $Si(SnMe_3)_4$ and $Ge(SnMe_3)_4$

Compounds $Si(SnMe_3)_4$ and $Ge(SnMe_3)_4$ represent yet another type of structural and dynamic solid-state properties. Below $T < 350$ K, high-resolution powder X-ray diffraction characterizes both compounds as ordered crystalline phases (space group $P\bar{1}$) and gives no indication as to the presence of dynamic disorder phenomena. $^{119}$Sn variable-temperature MAS NMR spectra confirm this finding and indicate a complete lack of molecular symmetry, with all four $SnMe_3$ groups per molecule being crystallographically inequivalent. The combined X-ray diffraction and solid-state NMR results contradict earlier interpretations of vibrational spectra of these compounds, which had been interpreted as indicating $T_d$ symmetry.[22] Variable-temperature $^{119}$Sn MAS spectra of $Ge(SnMe_3)_4$ are shown in Fig. 8. At a first glance these spectra seem to imply the presence of temperature-dependent dynamic exchange processes. However, $^{119}$Sn 2D EXSY MAS NMR experiments (at those temperatures where

 

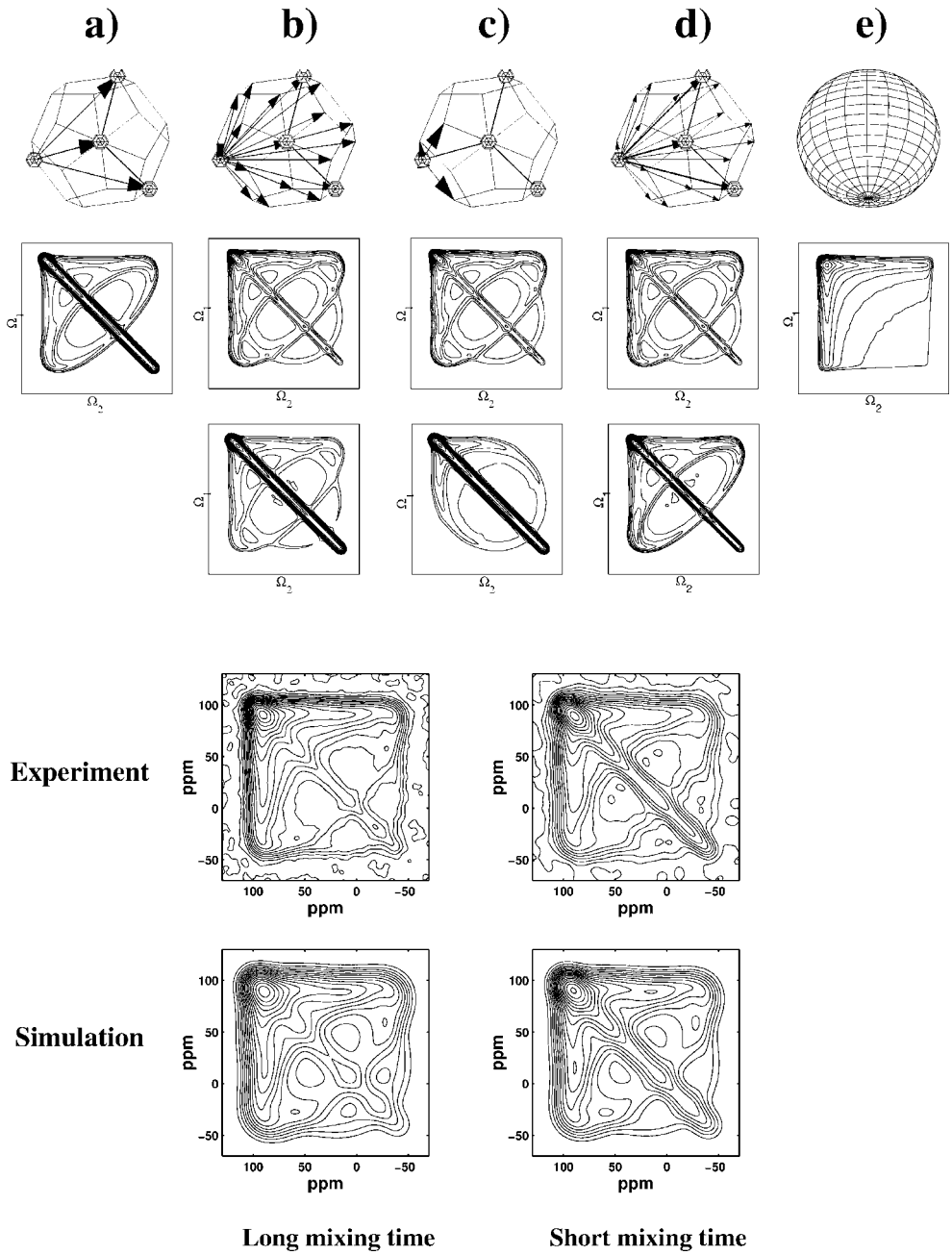


**Figure 7.** $^{119}Sn$ 2D EXSY experiments on a nonspinning sample, relevant as to the orientational disorder in $C(SnMe_3)_4$. Top half: columns (a) to (e) represent different orientational-disorder models as symbolized in the top row. The second row depicts the corresponding calculated contour plots of $^{119}Sn$ 2D EXSY experiments with mixing times long enough to ensure full exchange; the third row depicts contour plots of $^{119}Sn$ 2D EXSY experiments with short mixing times for models (b) to (d). Bottom half: contour plots of experimental (top) and best-fit simulated $^{119}Sn$ 2D EXSY experiments on $C(SnMe_3)_4$; model (b) with equal exchange rate constants for large- and small-angle jumps agrees best with the experimental data. See Ref. 3 for further details.

spectral resolution is observed) do not reveal any significant exchange. Accordingly, the small shifts (on the $^{119}Sn$ chemical shielding scale) and changes in the overall appearance of the $^{119}Sn$ MAS spectra of $Ge(SnMe_3)_4$ (and $Si(SnMe_3)_4$ as well) as a function of temperature have to be ascribed to intrinsic temperature shifts. The only remaining

 

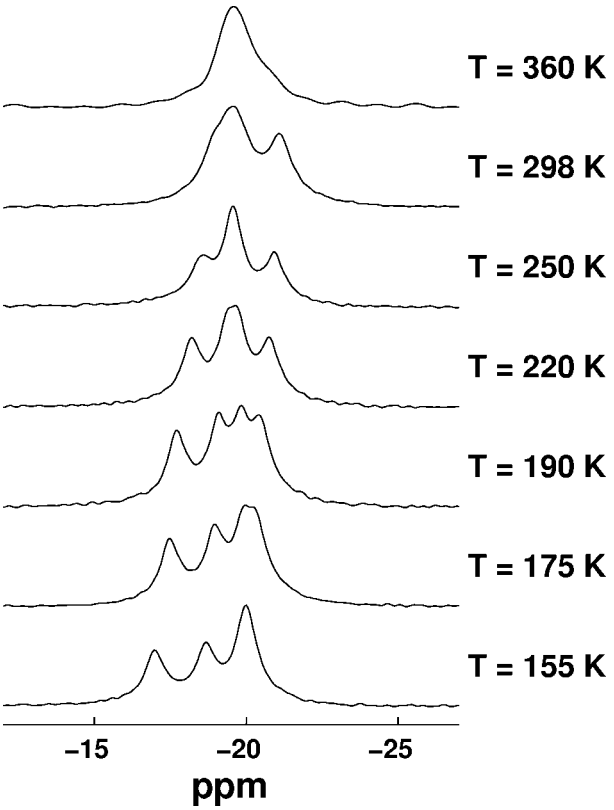


**Figure 8.** Variable-temperature $^{119}$Sn MAS NMR spectra of $Ge(SnMe_3)_4$ indicating lack of molecular symmetry and four crystallographically inequivalent $SnMe_3$ groups. The temperature-dependent effects in these spectra are solely due to intrinsic temperature shifts of the $^{119}$Sn isotropic chemical shielding values. See text and Ref. 4 for further details.

possible dynamic property of solid $Si(SnMe_3)_4$ and $Ge(SnMe_3)_4$ thus is internal reorientation of the individual $SnMe_3$ groups. Indeed, $^{13}$C 2D EXSY MAS experiments do indicate exchange amongst various methyl sites. However, given the lack of molecular symmetry, resulting in 12 methyl-$^{13}$C resonances per molecule, $^{13}$C MAS spectra of $Si(SnMe_3)_4$ and $Ge(SnMe_3)_4$ are not sufficiently resolved for any further in-depth analysis and quantification (in particular, the fact that crystallographically inequivalent groups $XMe_3$ in a molecule may show different rate constants of internal $XMe_3$ reorientation[23,24] would necessitate good spectral resolution as the basis of a meaningful analysis). The $^{119}$Sn MAS spectra depicted in Fig. 8 should serve as a reminder that reliable answers from straightforward MAS spectra, even regarding seemingly routine-type questions as to the multiplicity of sites or molecular point-group symmetry, may require recording of several spectra at different temperatures. A full account of the solid-state properties of $Si(SnMe_3)_4$ and $Ge(SnMe_3)_4$ is given elsewhere.[4]

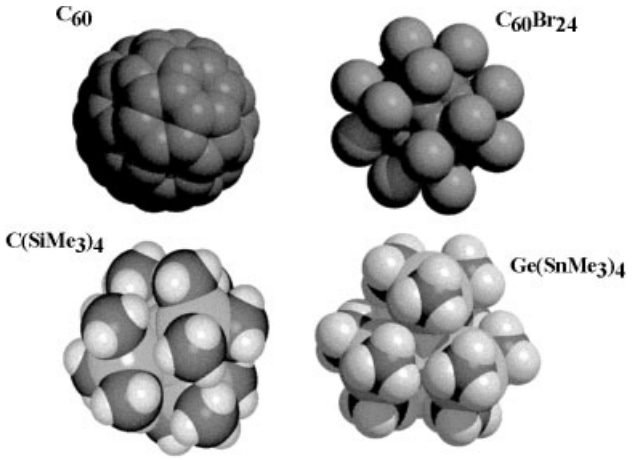


**Figure 9.** The molecular shapes of two members of the series of compounds $E(XMe_3)_4$ in comparison with the molecular shapes of their structure-and-dynamics counterparts from the group of fullerene, $C_{60}$, and its derivatives. See text and Ref. 4 for further details.

## SOME GENERAL COMMENTS

The members of the series of compounds $E(XMe_3)_4$ with E = C, Si, Ge and X = Si, Sn are chemical homologues of each other. Regarding the solid-state structures and dynamics, their properties are quite divergent. However, each member of the — chemically speaking — $E(XMe_3)_4$ family has its perfect structure-and-dynamics counterpart in a chemically very different class of compounds. For each of the compounds $E(XMe_3)_4$, a counterpart with identical disorder and phase-transition properties exists in the chemical group of fullerene, $C_{60}$, and its derivatives. Space-filling models of the molecular shapes such as those depicted in Fig. 9 illustrate the reasons for these cross-relationships amongst different classes of chemical compounds: shape matters; and even for largely nonpolar molecular solids, crystal packing appears to have more profound effects than one might be tempted to believe. In the future, recognizing and characterizing such interrelationships may help, for example, with the rational synthesis of composite materials or solid solutions. The *combined* use of high-resolution powder X-ray diffraction and solid-state NMR techniques has much to offer in this regard, much more than either of these complementary techniques could ever achieve on their own.

The focus of our discussion was a specific group of chemicals and a fairly narrow window of exchange rate constants of molecular dynamic solid-state properties. Neither are these or similar dynamic properties some special properties of compounds of the type $E(XMe_3)_4$, nor does the range of exchange rate constants encountered in this study represent the full range of molecular dynamics in organometallic solids and/or the full range of rate constants accessible to solid-state NMR. More often than not solid

organometallic compounds do display dynamic properties, and often the dynamics are not much slowed down compared with the solution state, with similar activation barriers. Typical examples are the properties of transition-metal complexes of aromatic $\pi$-bonded ligands or intramolecular CO exchange in transition-metal carbonyl complexes; for recent review articles, see Refs 25 and 26. In practical terms this means that solid-state NMR work on organometallic compounds will very often require variable-temperature NMR experiments, mostly at low temperatures. In particular, dynamic exchange processes with slightly higher rate constants than those we have enforced here (where necessary) by cooling of the samples will have additional effects on MAS NMR experiments. Molecular dynamics can interfere with the usually employed cross polarization (CP) step and make it very inefficient, to the extent that no CP response is obtained[27] and direct pulse excitation may become necessary. Or else, molecular dynamics may interfere with the $^1$H high-power decoupling and render the decoupling performance low,[28] or with the coherent averaging by the MAS, again leading to broad resonances.[29] In other words: if, under routine conditions at room temperature, you face difficulties in obtaining CP MAS NMR spectra, there is no reason to despair — you may have come across an interesting property of your sample rather than malfunctioning of the spectrometer (or the operator)!

## Acknowledgements

Financial support of our work by the Schwerpunktprogramm 'Silicium Chemie' of Deutsche Forschungsgemeinschaft and by Aventis, Paris, is gratefully acknowledged. We thank P. Bernatowicz, Warsaw, and J. Kümmerlen, Bayreuth, for their collaboration on some of the NMR parts of this project, and R. Dinnebier, Bayreuth/Stuttgart, for his continued cooperation regarding high-resolution powder X-ray diffraction investigations. The hospitality of the solid-state NMR laboratory at Nijmegen University, The Netherlands, made possible the low-temperature $^{119}$Sn NMR investigations on $C(SnMe_3)_4$, and G. Fritz, Karlsruhe, kindly donated our sample of $C(SiMe_3)_4$.

## REFERENCES

1. Helluy X, Kümmerlen J and Sebald A. *Organometallics* 1998; **17**: 5003.
2. Dinnebier RE, Dollase WA, Helluy X, Kümmerlen J, Sebald A, Schmidt MU, Pagola S, Stephens PW and van Smaalen S. *Acta Crystallogr. Sect. B* 1999; **55**: 1014.
3. Bernatowicz P, Dinnebier RE, Helluy X, Kümmerlen J and Sebald A. *Appl. Magn. Reson.* 1999; **17**: 385.
4. Dinnebier RE, Bernatowicz P, Helluy X, Sebald A, Wunschel M, Fitch A and van Smaalen S. *Acta Crystallogr. Sect. B* 2002; **58**: 52.
5. Abragam A. *The Principles of Nuclear Magnetism*. Oxford University Press: London, 1961.
6. Slichter C. *Principles of Magnetic Resonance*. Springer Verlag: Heidelberg, 1989.
7. Bennett AE, Griffin RG and Vega S. Recoupling of homo- and heteronuclear dipolar interactions in rotating solids. In *Solid-State NMR IV: Methods and Applications of Solid-State NMR*, Blümlich B (ed.). NMR Basic Principles and Progress, vol. 33. Springer-Verlag: Berlin, 1994; 1–78.
8. Dusold S and Sebald A. Dipolar recoupling under magic-angle-spinning conditions. In 'Annual Reports on NMR Spectroscopy', vol. 41, Webb G (ed.). Academic Press: London, 2000; 185–264, and references cited therein.
9. Ernst RR, Bodenhausen G and Wokaun A. *Principles of Nuclear Magnetic Resonance in One and Two Dimensions*. Clarendon Press: Oxford, 1992.
10. Sandström J. *Dynamic NMR Spectroscopy*. Academic Press, London, 1982.
11. Gerardy-Montouillout V, Malveau C, Tekely P, Oleander Z and Luz Z. *J. Magn. Reson. A* 1996; **123**: 7.
12. de Azevedo ER, Bonagamba TJ and Schmidt-Rohr K. *J. Magn. Reson.* 2000; **142**: 86.
13. van Gorkom LCM, Hook JM, Logan MB, Hanna JV and Wasylishen RE. *Magn. Reson. Chem.* 1995; **33**: 791.
14. Mildner I, Ernst H and Freude D. *Solid State Nucl. Magn. Reson.* 1995; **5**: 269.
15. Langer B, Schnell I, Grimmer AR and Spiess HW. *J. Magn. Reson.* 1999; **138**: 182.
16. Schmidt-Rohr K and Spiess H-W. *Multidimensional Solid-State NMR and Polymers*. Academic Press: London, 1994.
17. Meier BH. *Adv. Magn. Opt. Reson.* 1994; **18**: 1.
18. Bräuniger T, Poupko R, Luz Z, Zimmermann H and Haeberlen U. *J. Chem. Phys.* 2001; **115**: 8049.
19. Yang Y, Schuster M, Blümich B and Spiess HW. *Chem. Phys. Lett.* 1987; **139**: 239.
20. Ernst M, Kentgens A and Meier BH. *J. Magn. Reson.* 1999; **138**: 66.
21. Klinkhammer KW, Kühner S, Regelmann B and Weidlein J. *J. Organomet. Chem.* 1995; **496**: 241.
22. Leites LA, Bukalov SS, Garbuzova IA, Lee VY, Baskir EG, Egorov MP and Nefedov OM. *J. Organomet. Chem.* 1999; **588**: 60.
23. Helluy X, Kümmerlen J, Marschner C and Sebald A. *Monatsh. Chem.* 1999; **130**: 147.
24. Helluy X, Kümmerlen J and Sebald A. *Organometallics* 1997; **16**: 5218.
25. Aime S, Dastrù W, Gobetto R and Hawkes GE, Solid state NMR investigations of metal carbonyl complexes. In *Advanced Applications of NMR to Organometallic Chemistry*, Gielen M, Willem R, Wrackmeyer B (eds). Physical Organometallic Chemistry, vol. 1. John Wiley: Chichester, 1996; 159–192.
26. Duer MJ, Solid state NMR. In *Solid State Organometallic Chemistry, Methods and Applications*, Gielen M, Willem R, Wrackmeyer B (eds). Physical Organometallic Chemistry, vol. 1. John Wiley: Chichester, 1999; 227–278, and references cited therein.
27. Stejskal EO and Memory JD. *High Resolution NMR in the Solid State*. Oxford University Press: New York, 1994.
28. Rothwell WP and Waugh JS. *J. Chem. Phys.* 1981; **74**: 2721.
29. Suwelack D, Rothwell WP and Waugh JS. *J. Chem. Phys.* 1980; **73**: 2559.